

Mechanisms and Kinetics of WC-Co-Cr High Velocity Oxy-Fuel Thermal Spray Coating Degradation in Corrosive Environments

V.A.D. Souza and A. Neville

(Submitted June 20, 2005; in revised form August 2, 2005)

In this work, aspects of the corrosion behavior of WC-Co-Cr high velocity oxy-fuel (HVOF) thermal spray coatings have been assessed using a combination of x-ray photoelectron spectroscopy (XPS) and scanning electron microscopy (SEM) to understand the corrosion mechanisms and, in particular, the electrochemical interactions between phases. Direct current electrochemical accelerated corrosion techniques (potentiodynamic and potentiostatic tests) were performed to evaluate the corrosion kinetics of the coating. After the corrosion tests, the solution was analyzed using the inductively coupled plasma (ICP) technique, and a considerable amount of dissolved tungsten was detected. By combining information from XPS, SEM, ICP, and anodic polarization results, it is possible to propose a number of key reactions that can take place during WC-Co-Cr coating degradation, thus enabling the susceptible components of the coating to be identified. The implications of these findings for coating durability are discussed.

Keywords electrochemistry, high velocity oxy-fuel (HVOF), WC, x-ray photoelectron spectroscopy (XPS)

1. Introduction

The use of thermal spray coatings (TSC) has been expanded to include more applications than the original aerospace market, which dominated their use in the early days of their development. Among different coating processes, high velocity oxy-fuel (HVOF) has been very suitable for a number of applications due to the fact that it can provide coatings with very low porosity (less than 2%) and high wear resistance (Ref 1).

The use of HVOF WC-based coatings to improve the lifetime of materials has been very successfully achieved, as for instance, in the internal parts of centrifugal pumps, which in some cases have had their lifetime increased by 600% (Ref 2). Although HVOF WC-based coatings can provide wear resistance in erosion-corrosion environments, much is still to be done to understand the material degradation. Souza et al. (Ref 3) investigated the effect of corrosion of WC-Co-Cr HVOF coatings in erosion-corrosion environments, and it was reported that corrosion can be a dominating mechanism. In Fig. 1, the components of degradation in an erosion-corrosion environment for WC-Co-Cr HVOF coatings have been categorized as mechanical erosion (E) and corrosion-related damage ($C + S$), where C is the in situ corrosion rate in erosion-corrosion and S is the effect of corrosion in enhancing the erosion degradation. The segregation of components of damage by this approach has been previously reported for a range of materials in Ref 4-7. The numbers 1, 2, and 3 are related to the sand loading used in the experiment—200, 500, and 1000 mg/l, respectively—whereas the circles are

the results at 20 °C and squares at 50 °C. Also, the damage components for UNS S327650 at 20 °C are presented to have a comparison. From this, it is clear that the HVOF coatings in an erosion-corrosion environment are placed near the line separating the corrosion-dominated regimen from the erosion-dominated regimen, and in this respect corrosion is an important issue. Also, there may be applications in which coatings are required to operate in an aqueous environment for long periods, and therefore static corrosion considerations are often vital in material selection.

In this work, the corrosion behavior of WC-based coatings has been categorized into two key processes, and each has been considered in detail:

- (a) Corrosion of matrix and release of WC particles by loss of the supporting matrix (Ref 8-12)

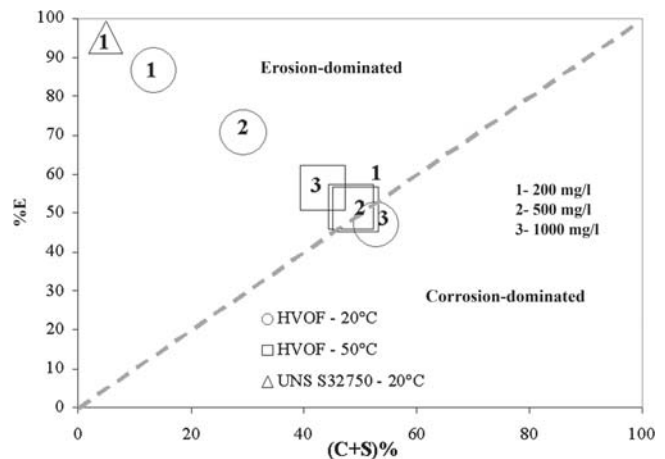
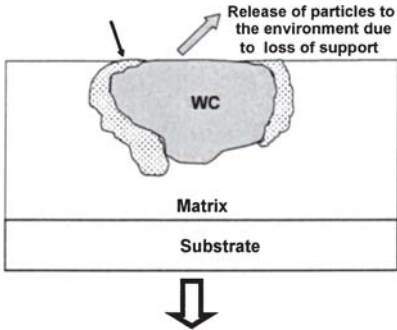
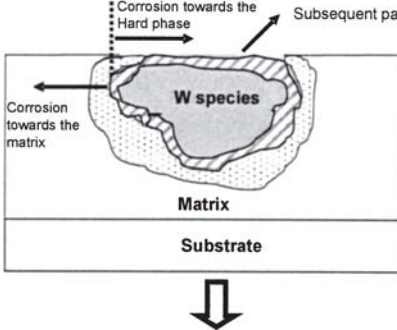


Fig. 1 Dominant regime of HVOF WC-Co-Cr coatings under erosion-corrosion environments (Ref 3)

V.A.D. Souza and A. Neville, School of Mechanical Engineering, University of Leeds, Leeds LS2 9JT UK. Contact e-mail: a.neville@leeds.ac.uk.

Table 1 Key processes considered in corrosion of WC-based coatings

Corrosion of matrix	Corrosion of hard phase and matrix
	
<p>Human et al. (Ref 8): Leaching of Co leaving WC skeleton Human et al. (Ref 9): Corrosion behavior of Co and Co(W,C) in 1 N sulphuric acid Monticelli et al. (Ref 10): Dissolution of Co in HVOF WC/Co is enhanced by WC due to galvanic effects Truman et al. (Ref 11): Detection of Co and Fe after electrochemical test in MMC using atomic absorption but no tungsten Wentzel et al. (Ref 12): WC particle is pulled out in slurry environments</p>	<p>Scholl et al. (Ref 13): Presented the oxidation of WC as a function of potential Ghandehari (Ref 14): Dissolution of Co and WC of cemented WC6Co alloy Tomlinson et al. (Ref 15): Dissolution of WC after anodic polarization of cemented carbides Imasato et al. (Ref 16): Dissolution of WC from WC-Ni-Cr3C2 Ebara et al. (Ref 17): Oxidation and dissolution of WC in HVOF WC based coatings</p>

(b) Corrosion of WC particles and matrix, loss of WC also being an electrochemical process (Ref 13-17)

The idea of corrosion of matrix and subsequent release of the hard phase has always been considered to be the main mechanism of WC-based cermet materials as pointed in (a), whereas for (b) only recently have both the corrosion of WC (hard phase) and the matrix been in the level of detail required to obtain full understanding of the corrosion processes involved. In this work, both mechanisms were considered through a review of the main findings from some important works, as presented in Table 1.

The corrosion behavior of individual components in cermet materials such as WC could provide some more information on how the material degrades in different environments, and Table 2 shows a summary of some of the key papers in this area of WC powder oxidation and dissolution (Ref 18-23).

This paper has as its main objective the determination of kinetics and mechanisms of corrosion of a HVOF WC-Co-Cr coating in static saline solution realizing the importance of the interactions between the components and also the importance of corrosion in relation to degradation in erosion-corrosion.

2. Experimental Procedure

2.1 Sample Preparation and Characterization

The samples for electrochemical monitoring were 1×1 cm coupons. The samples as-received were ground, carried out on a Kallenburg Surface Grinder (Alfred Herbert Ltd., Coventry, UK). The samples were held in a magnetic rotary chuck and ground individually to minimum clean-up with a diamond cup wheel and to obtain the final finish, items were lapped on a rotary lapping table to achieve both flatness and finish. The coating was applied using a commercial HVOF system (G-Gun,

Table 2 Corrosion of WC powder

Authors	Findings
Warren et al. (Ref 18)	WC oxides in air with relative humidity of 60-95% while in water no oxide at all was visible
Voorhies (Ref 19)	Oxidation of WC into WO_3 with formation of WO_3 hydrate
Andersson et al. (Ref 20)	Oxidation of WC into WO_3 and dissolution of WO_3 into WO_4^-
Bozzini et al. (Ref 21)	Oxidation of WC into WO_3
Papazov et al. (Ref 22)	Oxidation of WC depends mainly on WC specific surface area
Nikolov et al. (Ref 23)	Oxidation of WC is related to type of material used for WC synthesis

Greenhey Ltd, Lancashire, UK). The coating porosity was specified to be less than 1.0%, and the coating thickness was 250 μ m.

All samples were ground with 1200 grit SiC paper and finally polished using a 6 μ m diamond paste. They were then encapsulated in a nonconducting epoxy resin with the rear side of the specimen soldered to a wire. Specimens were examined prior to testing to characterize the microstructure and after corrosion tests to establish the corrosion mechanisms using a scanning electron microscope (SEM) with an energy dispersive x-ray (EDX) chemical analysis device, which provided quantitative correction procedures for atomic number, absorption, and fluorescence (ZAF). The specimen-resin interface of the encapsulated specimen was painted with a sealing lacquer, Lacomit Varnish-Agar Aids (Sutton Tools, Birmingham, UK), to prevent interference in the electrochemical measurements from the substrate material. X-ray photoelectron spectroscopy (XPS) was performed in a Scienta ESCA 300 at National Centre for Electron Spectroscopy and Surface Analysis (NCESS), Daresbury, UK laboratory. Etching by an argon-ion beam was done for dif-

ferent periods to probe the surface composition as a function of depth. Where a bulk analysis of the coating was required, a long etching time of several minutes was used. Where the near surface features were of interest, no etching was used initially, and then the etching time was progressively increased to build up a depth profile. Etching was conducted at 2 kV. The absolute values of binding energies were referenced against the C 1s peak, taken to be 284.88 eV.

2.2 Electrochemical Corrosion Measurements

2.2.1 Potentiodynamic Tests. The corrosion behavior in static conditions was assessed by direct current (dc) potentiodynamic polarization tests in 3.5% NaCl. Anodic polarization tests were carried out at different temperatures. These polarization tests involved using a standard three-electrode electrochemical cell as shown in Fig. 2, and the sample area was within the range of 0.5–1 cm². The computer controlled potentiostat (Solartron 1280, Durham, UK) was used to shift the potential of the working electrode (the specimen) relative to the reference electrode (saturated calomel electrode-SCE) at a predetermined rate of 15 mV min⁻¹ to potentials more positive than the free corrosion potential (E_{corr}). The current density in the external circuit between the Pt auxiliary electrode (AE) and the coating (working electrode, WE) was measured as a function of applied potential until the current density of 500 $\mu\text{A}/\text{cm}^2$ was reached and then the potential would drop at the same rate as on the forward curve. Where appropriate, corrosion rates were determined by the Tafel extrapolation technique (Ref 24).

2.3 Inductively Coupled Plasma Analysis

The inductively coupled plasma (ICP) analysis of the solution was performed with a JY 138 Ultrace model, which is a sequential emission spectrometer from Jobin Yvon Horiba (Middlesex, UK). It enabled the concentration of dissolved Co, Cr, and W ions in the solution to be determined. The calibration was performed with starting spectroscopic solutions diluted in 3.5% NaCl: ammonium tungstate $[(\text{NH}_4)_2\text{WO}_4]$ in water, chromium (iii)nitrate $[\text{Cr}(\text{NO}_3)_3 \cdot 9\text{H}_2\text{O}]$ in nitric acid (HNO_3), and cobalt (ii)nitrate $[\text{Co}(\text{NO}_3)_2 \cdot 6\text{H}_2\text{O}]$ in nitric acid (HNO_3).

3. Results and Discussion

3.1 Coating Composition and Microstructure

In this work, the WC-Co-Cr (86% WC, 10% Co, 4% Cr) HVOF coating was studied. The EDX and XRD analysis for this coating were presented in Ref 3, 25, which confirmed that the coating is 86% WC, 10% Co, and 4% Cr with sharp peaks of WC and a small amount of W_2C .

Figure 3 shows the SEM backscattered image of the microstructure of the coating in the as-polished condition with the tungsten carbide particles showing a clear angular shape and uniform particle distribution over the surface.

3.2 Electrochemical Tests

The complexity of corrosion of WC-Co-Cr HVOF coatings has already been presented in Ref 3, 25, where it was shown that

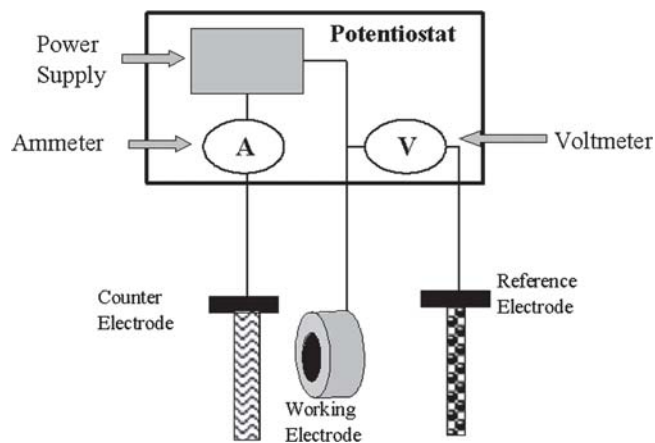


Fig. 2 Three electrode cell used in the electrochemical experiments

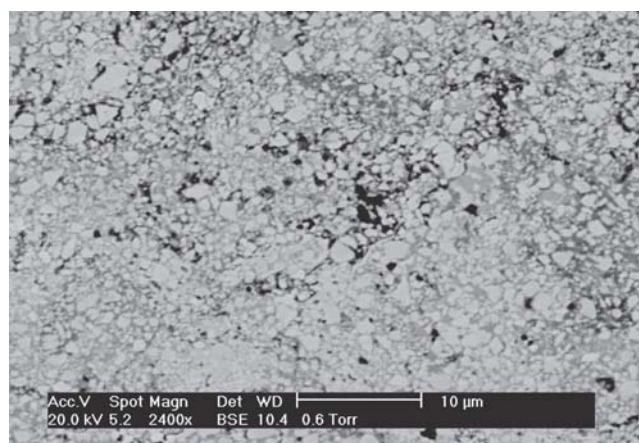


Fig. 3 SEM image of the as-polished WC-Co-Cr coating surface

the coating presented a passive-like behavior after anodic polarization at 18 °C and also two values of breakdown potential in contrast to stainless steel, which presents a clear passive region and breakdown potential. In this paper, a comprehensive analysis of corrosion is shown the corrosion response through anodic polarization curves at different temperatures (Fig. 4). The behavior at 18 °C is a passive-like behavior, but the current is higher than a typical passive material (1 $\mu\text{A}/\text{cm}^2$), such as stainless steel. Passive behavior is characterized by thin film formation, which protects the surface against any charge transfer, and consequently corrosion and the breach of this passive film in an anodic polarization appears as a rapid increase in current density at a certain potential (breakdown potential). Furthermore, at 18 °C, the curve presents two values of breakdown potential (0.6 and 0.8 V) whereas at 30 and 50 °C, a higher current density is reached, and the breakdown potential is reduced, showing less resistance to charge transfer. The presence of two values of breakdown potential indicates that at 0.6 V, the corrosion of WC takes place (Ref 14) and at 0.8 V, the increased current is likely to be associated with WO_3 formation and a contribution from the oxygen evolution or transpassive dissolution reactions involving Cr oxide film rupture (Ref 13, 26). However, the behavior of the curves 70 and 90 °C is completely active, indicated by the rapid increase of current density from the open circuit potential (E_{corr}).

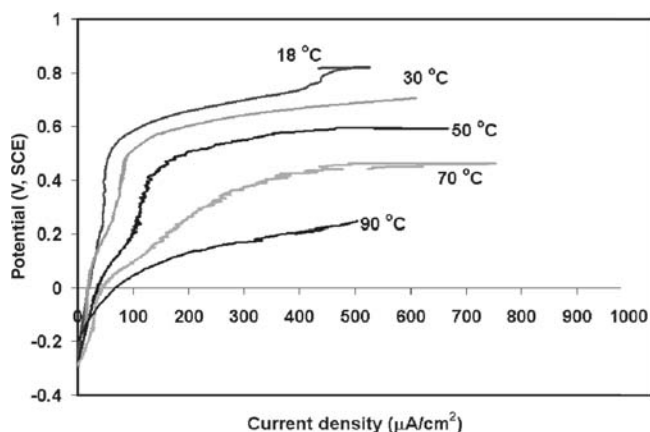


Fig. 4 Anodic polarization of WC-Co-Cr coating at different temperatures in 3.5% NaCl in static conditions

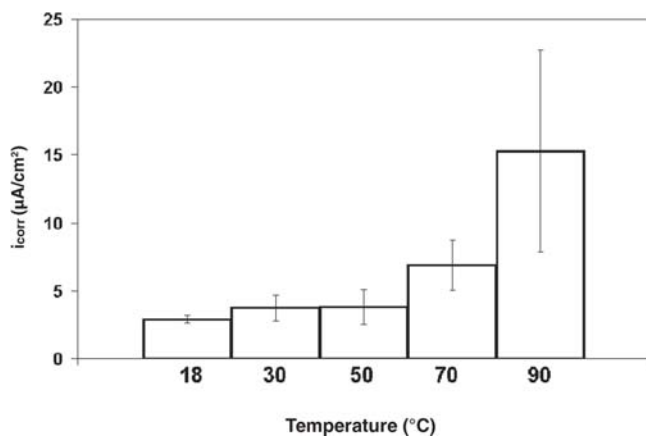


Fig. 5 Corrosion current density of HVOF WC-Co-Cr coating at different temperatures in 3.5% NaCl in static conditions

The corrosion rate (i_{corr}) (Fig. 5) shows a strong dependence on temperature.

SEM images after anodic polarization at 18 and 50 °C are shown in Fig. 6 and 7. These figures show that the attack initiates mainly at the interface between hard phase and matrix. A white contour with the same shape as tungsten carbide particles represents regions where hard phase removal has taken place. It is also important to mention that very small particles (<0.5 μm) seem to have been completely removed from the surface.

The following sections will present the XPS results and also the ICP analysis of the solution after anodic polarization in different conditions.

3.3 XPS Results for Samples As-Polished and After Anodic Polarization at 18, 50, and 90 °C

To detect any phase transformation on the surface after anodic polarization XPS analysis, which can provide information on the upper 10 nm of the surface, was performed on the samples as-polished and after anodic polarization at different temperatures. Also, to understand more about the corrosion mechanisms, some XPS analysis was performed on samples submitted to anodic polarization and stopped at different potentials.

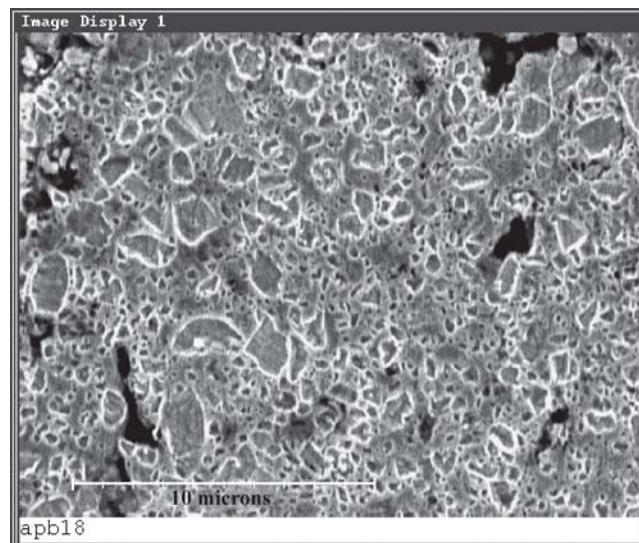


Fig. 6 SEM image after anodic polarization at 18 °C

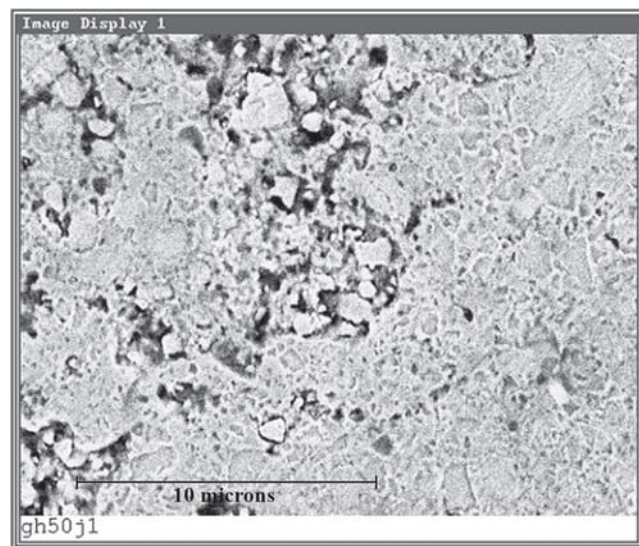


Fig. 7 SEM image after anodic polarization at 50 °C

In XPS analysis, it is important to understand the aim of etching a sample, as for this work, etching means bombarding the sample with ionized argon and this could change the surface features of the WC-Co-Cr. Etching the surface before performing the XPS analysis is a way not only to remove the undesirable compounds (grease, dust) from the surface, but also to observe the different oxides or phase layer change along the depth. In this work, three different etching procedures were used to obtain the specific information. On the as-polished samples, the interest was on the bulk composition and phase characteristics of the material, and therefore a 30 min etching was chosen, whereas the etching time after anodic polarization tests was set at 15 min, as will be discussed later. Another series of XPS tests were performed on samples submitted to anodic polarization stopped at different potentials, and in these tests, no etching was performed to avoid any loss of information on the very surface of material.

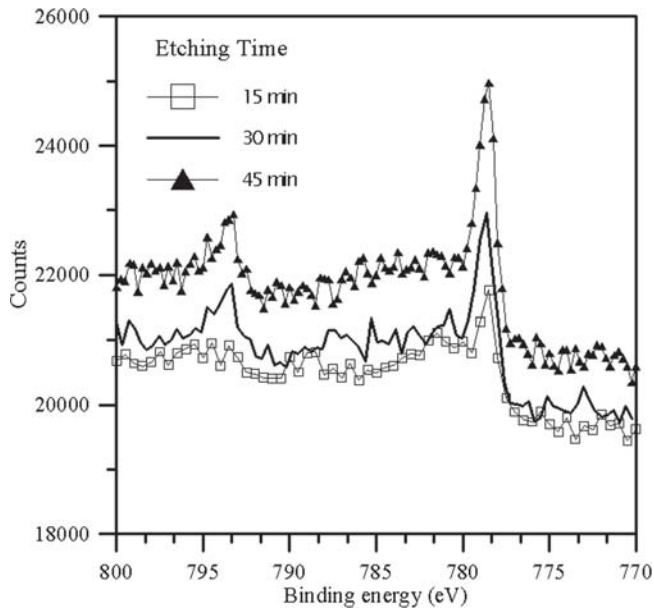


Fig. 8 XPS analysis of Co 2p after anodic polarization at 18 °C at three different etching times (15, 30, and 45 min)

To evaluate the effect of etching time on WC-Co-Cr surface features after anodic polarization, the tests were performed at 15, 30, and 45 min, as shown in Fig. 8 for Co 2p. The Co metal has a binding energy of 778.1 eV and according to Souza (Ref 26), it is essential to analyze the material at different etching times to be able to detect surface layer transformation for samples submitted to anodic polarization tests. Fifteen minutes etching seems to provide better information on the surface changes rather than 30 or 45 min, as they go deeper in the coating, and for this reason, the following XPS results will be presented with 15 min etching time after anodic polarization. However, the time of 15 min adopted in this work does not mean that it is the optimum etching time for evaluating HVOF coatings after anodic polarization, which should be investigated in greater depth.

Figure 9 shows the XPS results for Cr before and after anodic polarization, and it is observed that the peak for Cr₂O₃ has an intensity similar to that of the Cr metal peak in the as-polished sample. The XPS spectrum for Cr 2p after 30 min etching on the as-polished samples shows the doublets associated with Cr metal and Cr₂O₃ are apparent at 574.49 and 576.78 eV, respectively. This shows the presence of a thin Cr₂O₃ layer on the surface of the coating, evidence that the Co/Cr matrix has sufficient Cr to develop a passive film.

However, for samples after anodic polarization, the Cr₂O₃ peaks are much more pronounced than the Cr metal peaks, indicating that Cr₂O₃ has become thicker and so with the same analysis depth (15 min etching time) a higher oxide/metal ratio is recorded.

Figure 10 shows that the intensity of the Co 2p metal peaks at 778.1 eV is reduced after anodic polarization at 18 °C and is further reduced at higher temperatures. In addition, after anodic polarization, there is a small amount of Co oxide detected as a small peak at 781.2 eV when compared with the as-polished, which presents the metal peak at 778.1 eV.

Figure 11 shows the W 4f XPS peaks, and it is observed that

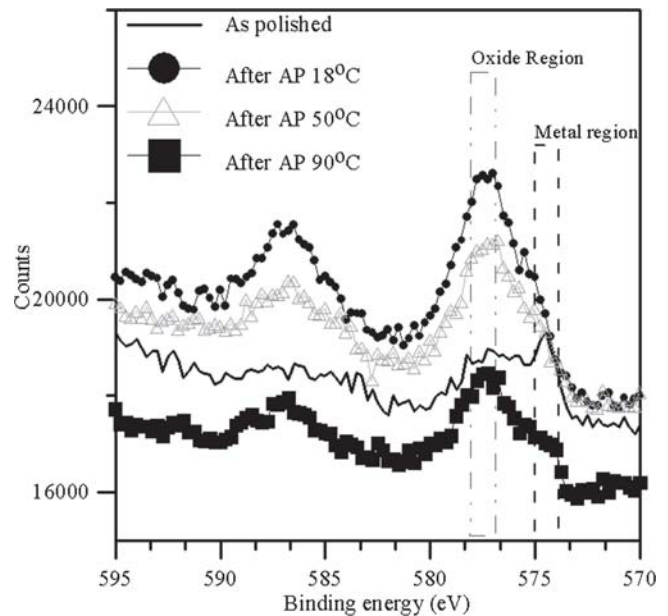


Fig. 9 XPS analysis of Cr 2p as-polished (30 min etching) and after AP at 18, 50, and 90 °C (15 min etching time)

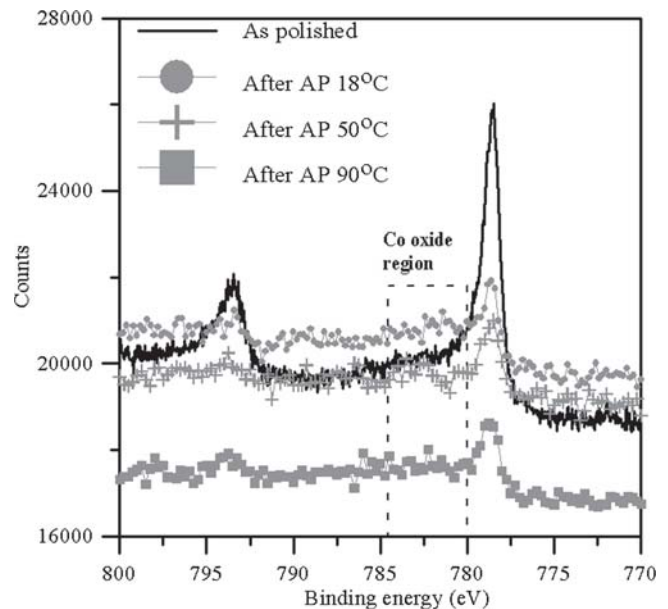


Fig. 10 XPS analysis of Co 2p as-polished (30 min etching) and after AP at 18, 50, and 90 °C (15 min etching time)

on the as-polished sample WC peaks has a high intensity while WO₃ presents a small peak between 35 and 40 eV. However, the amount of WO₃ (most predominant tungsten oxide specie) (Ref 27-29) increases after anodic polarization at 18 and 50 °C but drops at 90 °C at 40-35 eV. Another fact is that the WC peaks present lower intensity as the temperature of anodic polarization increases, which could be related to the chemical removal of WC during anodic polarization.

Analysis of XPS results enables a series of transformation of different species on the surface of WC-Co-Cr HVOF after an-

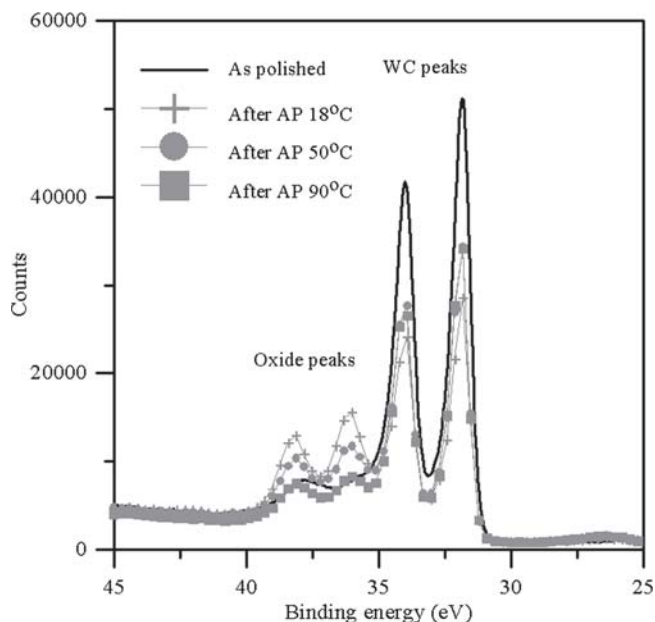


Fig. 11 XPS analysis of W 4f as-polished (30 min etching) and after AP at 18, 50, and 90 °C (15 min etching time)

odic polarization tests to be identified and assessed. Also, the effect of temperature in these transformations is evident. Table 3 presents a summary of the changes on the ratio of oxide/metal species for Co, Cr, and W.

3.4 XPS as a Function of Potential

To evaluate the phase transformations in the WC-Co-Cr coating during electrochemical tests, different samples were subjected to anodic polarization tests, where the tests were stopped at different potentials and then analyzed by XPS. The anodic polarization tests were performed on two samples stopping at $0.0 V_{SCE}$ and at $0.8 V_{SCE}$ on the forward curve, as presented in Fig. 12. After the tests were stopped, the samples were rinsed with distilled water, dried with compressed air, and taken to XPS with no etching to detect changes at the very outer surface of the material. The fact that not having etched the surface of HVOF coatings can be explained by trying to detect the predominant formation of WO_3 , which can be easily removed or ionized by the etching fluid.

Figure 13 shows the XPS analysis for Co 2p as a function of potential. The interesting effect occurs at $0.0 V_{SCE}$ with the detection of cobalt oxides next to the metal peak as an intermediate reaction and also indicative of a weak passive layer formation. Recent work by Sutthiruangwong et al. (Ref 30) on passivity and pseudopassivity of cemented carbides demonstrated that when commercial cemented carbides with 8% Co content and 0.7% Cr_3C_2 addition (WCCo8-07Cr) are polarized at $100 mV_{SCE}$ for 1 h, a mixed CoCr oxide layer is considered as a true passive layer; this was confirmed by transmission electron microscopy (TEM). According to Milosev et al. (Ref 31), the cobalt metal ($2 p_{3/2}$) presents a peak at 778.1 eV (width 1.45) and the oxide group ($CoO + Co_2O_3/Co_3O_4$) at 780.5-781.2 eV (width 3.3 eV), where it was pointed out that the binding energy for the oxides is very

Table 3 Summary of changes after anodic polarization at 18, 50, and 90 °C for Co 2p, Cr 2p, and W 4f

Component	Changes after anodic polarization (compared to as-polished surface)
Co	Reduction of Co metal peaks and formation of oxide species
Cr	Higher oxide/metal as the temperature increases
W	Higher oxide/metal at 18 and 50 °C and lower at 90 °C

close, and that they can overlap, making it difficult to distinguish the type and amount of each cobalt oxide formed.

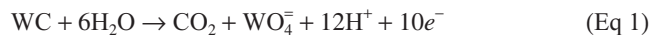
The XPS results for W 4f at different potentials are shown in Fig. 14. At $0.0 V_{SCE}$, WC peaks are more intense than WO_3 peaks, which are similar to the results given in Fig. 11 for the as-polished surface. At $0.8 V_{SCE}$, which was close to the current density reverse point ($500 \mu A/cm^2$), the tungsten oxide (WO_3) peaks are higher than tungsten carbide peaks.

3.5 ICP Tests

Figure 15 shows the ICP analysis for tungsten and cobalt in the solution after anodic polarization at different temperatures in the 3.5% NaCl solution. The concentration of W in the solution is much higher than Co, whereas Cr^{3+} is not detectable in the solution after the tests. The reason for this can be related to Cr_2O_3 formation after anodic polarization preventing Cr from dissolution, as will be shown in a later section of this work. Combining information from Fig. 3, 6, and 7, it is possible to see that the corrosion process is complex. Comparing Fig. 3 with Fig. 6 or 7 it is clear that some small WC particles have been removed and the detection by ICP of a considerable amount of $[WO_4^-]$ in the solution indicates that WC particles have been chemically removed. The chemical removal of WC small particles could be assisted by the electrochemical dissolution of the binder alloy, which in spite of the formation of passivating Cr oxide, is demonstrated by the amount of Co detected by ICP analysis, which seems to be equal or higher than 10% of the dissolved composite.

To check whether the amount of W detected in the solution through ICP (WC dissolution) matches the density of “voids” (WC removal) seen in SEM images after anodic polarization, an estimate analysis was performed as follows.

The calculation of the amount of WC in the solution after anodic polarization was performed, first correcting the amount of $[WO_4^-]$ from the ICP results (ppm) to the volume used for the experiments (200 ml). Secondly, the amount of WC was obtained using the stoichiometry of reaction 1 (Ref 14, 16) where the mass of WC is calculated from $[WO_4^-]$:



The calculation of the amount of WC chemically removed from the surface using SEM was performed determining the number of “voids” present in an area of $100 \mu m^2$, which can be distinguished by the “black regions” on the surface as presented by Fig. 6. In this calculation, the “voids” are assumed to be spherical and the average diameter between 0.5 and $1.0 \mu m$. The result is then extrapolated for the whole area of the sample surface used in the experiments ($0.4 cm^2$) and presented in Fig. 16.

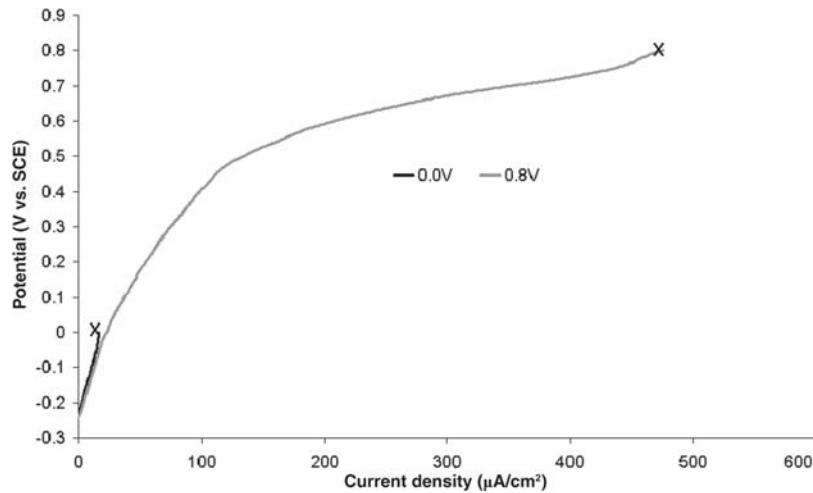


Fig. 12 Anodic polarization tests stopped at 0.0 V and 0.8 V and taken to XPS analysis

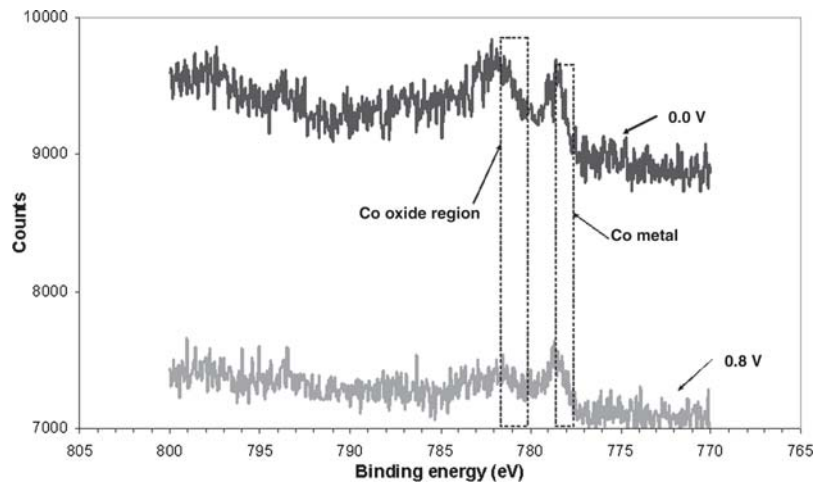


Fig. 13 XPS results for Co 2p after anodic polarization stopped at 0.0 and 0.8 V_{SCE} at 18 °C

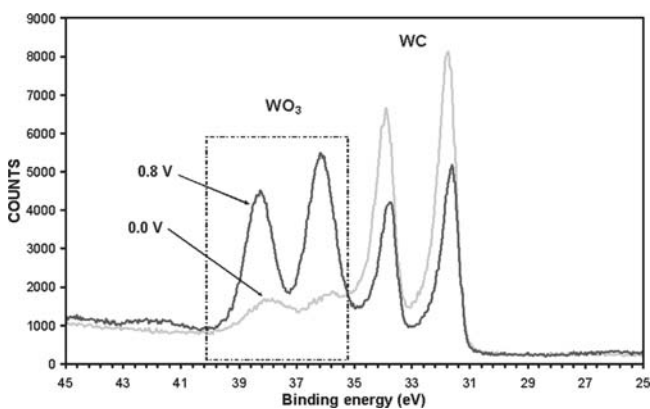


Fig. 14 XPS results for W 4f after anodic polarization stopped at 0.0 and 0.8 V_{SCE} at 18 °C

The difference between mass loss of WC calculated through ICP and SEM could be related not only due to the assumptions already made but also due to a non-uniform corrosion process,

which takes place over the whole surface area of 0.4 cm^2 and the formation of WO_3 that remained on the surface. Another reason for the difference could be attributed to the release of WC into the solution, which could accentuate the higher values for the SEM results. The key point is that there is generally good compatibility of the results showing that the mass losses between the two calculations are comparable.

If all of the dissolution of the coating leads to formation of soluble species in the solution, the amount of species in the solution will be proportional to the charge (Q) generated during anodic polarization, since $Q = \int i dt$ (where i is the current density and t is time). In Fig. 15, it is shown that the charge is not always directly proportional to the amount of species in the solution, which indicates that part of the charge transfer excess might have been consumed to form chromium oxide or there was enough charge built to break the film and form CrO_4^- and Cr_2O_7^- , which were not analyzed by ICP (Ref 26).

Figure 17 shows the determination of i_{\max} in the anodic polarization curve for WC-Co-Cr HVOF and stainless steel UNS S31603 at 18 °C, and Fig. 18 shows the i_{\max} results for HVOF

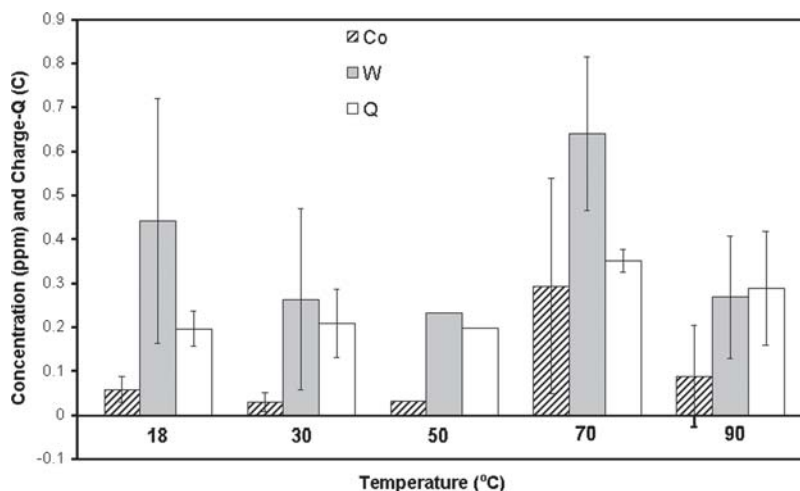


Fig. 15 ICP analysis for W and Co and charge generated (Q) after anodic polarization at 18, 30, 50, 70 and 90 °C in 3.5% NaCl solution

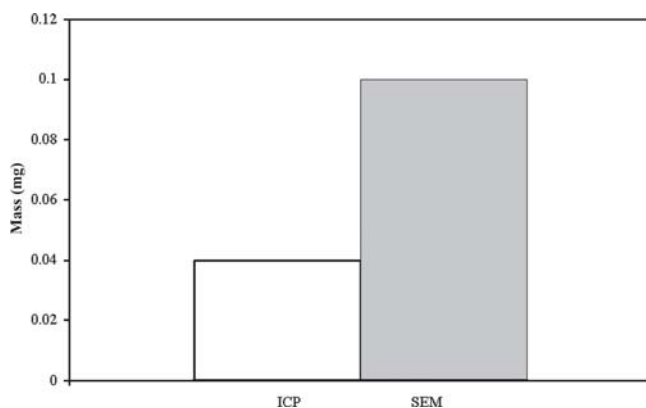


Fig. 16 Comparison of WC mass loss by calculation through ICP and SEM

WC-Co-Cr coating at different temperatures. The i_{\max} represents the propagation of corrosion, which is translated by the increase of current even when the potential is reduced. The reduction of the potential occurs when the current density reaches a predetermined value of $500 \mu\text{A}/\text{cm}^2$. At this current density, the potential starts dropping, and recovery of any possible passive film is likely to occur. The low values of i_{\max} in Fig. 18 for WC-Co-Cr HVOF coatings compared with stainless steel (UNS S31603) in Fig. 17 also indicate that HVOF WC-Co-Cr coatings are not likely to form pits, which propagate as occluded regions and repassivate with great difficulty.

This effect shows the inertia of corrosion propagation as well as the capacity of the surface to recover when potential films are likely to reform. Therefore, the value of i_{\max} is likely to be related to the surface conditions, ability to repassivate, and activation energy necessary to initiate certain reactions.

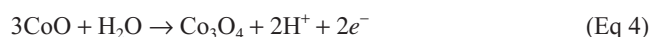
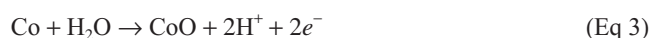
The information provided by the charge generated during anodic polarization tests, and the i_{\max} suggests that some intermediate reactions take place with the formation of different oxides, and to be able to propose some sequential reactions, the combination of XPS, ICP, and SEM after anodic polarization information should be considered and performed.

It has been reported (Ref 25), that relating ICP results as a function of potential indicates that cobalt starts dissolving before tungsten, according to the following reaction:



This reaction is believed to take place rapidly up to $0.05 V_{\text{SCE}}$, and it is reduced up to $0.5 V_{\text{SCE}}$ according to Ghandehari (Ref 14). The reduction of cobalt dissolution between 0.05 and $0.5 V_{\text{SCE}}$ could be associated with oxide formation as reported by Ohtsuka et al. (Ref 32), where it was stated that at pH 8.4, cobalt forms oxide. In fact, the formation of oxide after anodic polarization can be observed in Fig. 13, supporting this hypothesis.

The formation of cobalt oxide takes place at low potentials, for instance at $0.0 V_{\text{SCE}}$ (Ref 32), and it reduces at higher potentials (0.8 V) as presented by Fig. 13. The predominance of cobalt oxide takes place mainly at 0.0 V according to the following possible reactions:



Cr_2O_3 peaks have higher intensity after anodic polarization at 18°C , as presented in Fig. 9. The reduction of the Cr_2O_3 peak intensity at 50 and 90°C could also be related to the detachment of Cr oxides from the surface, which could also form Cr in different oxidation states rather than Cr^{3+} , which is the state that was analyzed by ICP in this work. Also, the Cr_2O_3 peaks after anodic polarization at 50 and 90°C are still slightly higher than those on the as-polished sample showing the increase of Cr_2O_3 formation.

WO_3 can be present on the as-polished surface or formed after anodic polarization at 18°C as presented by XPS results. The dissolution of WO_3 , which is another source of W, can be

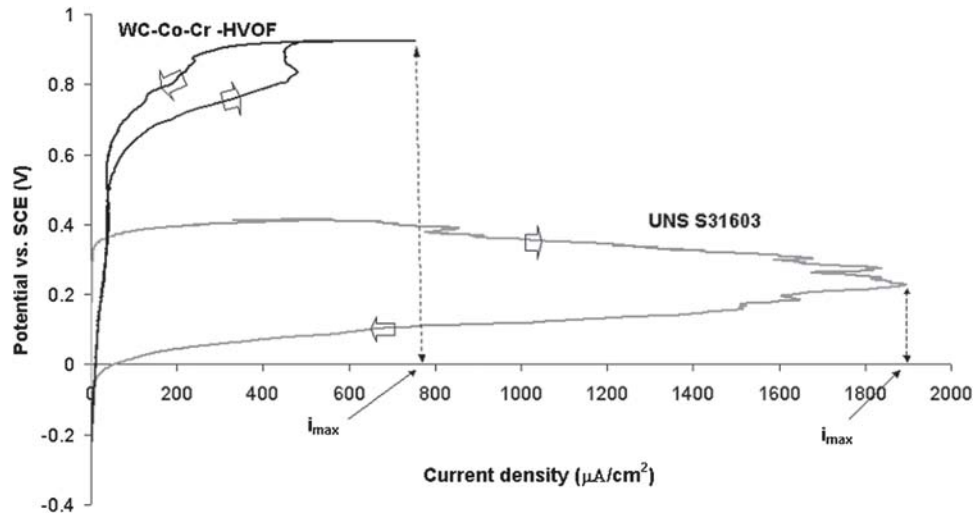


Fig. 17 i_{\max} representation in anodic polarization curves of WC-Co-Cr HVOF and UNS S31603 at 18 °C

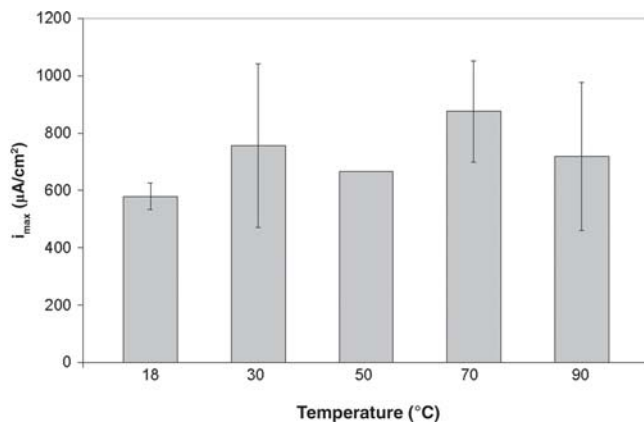
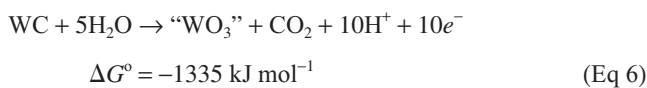
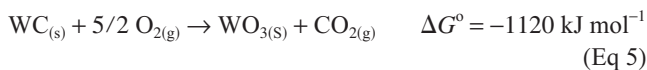


Fig. 18 i_{\max} as a function of temperature for HVOF WC-Co-Cr at different temperatures

demonstrated by consulting the Pourbaix diagram (Ref 33) in Fig. 19, indicating that WO_3 in water dissolves at pH higher than 4.

However, WO_3 is not only present on the as-polished surface but also is formed after anodic polarization as shown by XPS. The formation of WO_3 after anodic polarization indicates a possible intermediate reaction at some sites before dissolution into $[WO_4]^-$. The oxidation of WC has been shown to be thermodynamically possible as observed by the estimated Gibb's free energy for two different reactions as follows (Ref 19, 20):



WO_3 can be formed and present on the surface or solution in different species, as reported by Firman et al. (Ref 27) in the

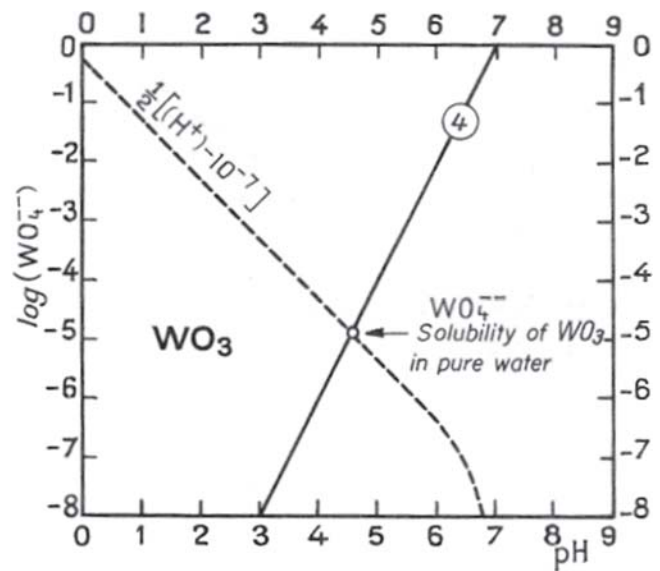


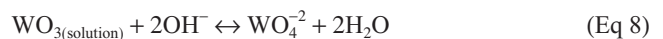
Fig. 19 Solubility of WO_3 in water (Ref 33)

investigation of W dissolution in alkaline hydroxide and sodium carbonated solutions. The stoichiometry of the reversible dissolution reaction can be presented as follows:



Also, the $WO_3(H_2O)_{\text{surface}}$ could be formed.

It was theorized that the dissolution of WO_3 in alkaline solution was followed by a much slower reaction to the more thermodynamically stable species:



WO_3 can also be found in acid environments and the dissolution occurs via formation of WO_2^{2+} surface species (Ref 28) and also

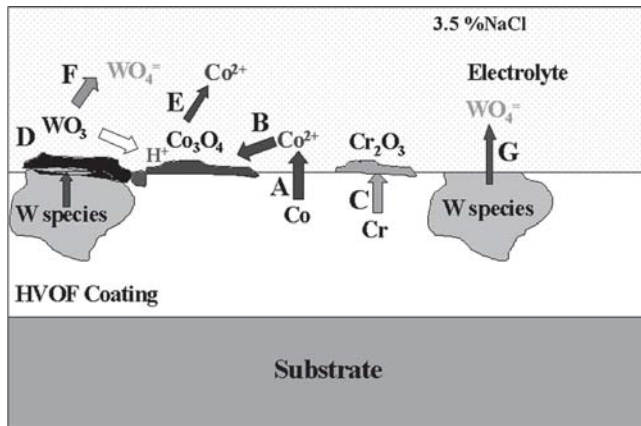
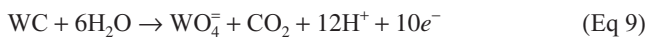


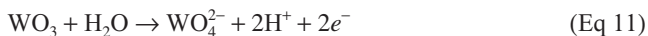
Fig. 20 Summary of corrosion mechanisms for WC-Co-Cr HVOF coating suggested in this work

in similar environments the W forms a protective oxide (W_2O_5). These facts indicate that in this work the WO_3 formation and dissolution is complex and depend on the localized environment.

The reaction for WC is initially thought to be only the dissolution to $[WO_4^-]$ but as some authors mentioned before (Ref 13-14, 17, 19) WC goes through oxidation (WO_3 formation) and then dissolution $[WO_4^-]$. Because of the complexity of corrosion of WC-based coatings it is believed that in some areas of the surface, WC can dissolve without going through the oxidation step, as presented by reaction (9) and this fact could be associated with the potential.



The XPS results at $0.8 V_{SCE}$ in Fig. 14 and ICP results in Fig. 15 indicate that WC goes through oxidation and dissolution via the following reaction steps:



Reactions (10) and (11) appear to take place at a certain potential (0.6-0.8 V); at this potential, the formation of WO_3 suggests that the pH around the WC particle drops and as a consequence the cobalt oxide remaining is dissolved as stated by Sato et al. (Ref 32) and shown in reaction (12):



This interaction between Co and WC could be one of the reasons that interface corrosion attack at the WC/matrix boundary occurs as an initiation process.

3.6 Sequence Reaction Mechanisms of WC-Co-Cr Corrosion

To summarize the corrosion mechanisms of the WC-Co-Cr HVOF coating as well as the sequence of the reactions, Fig. 20

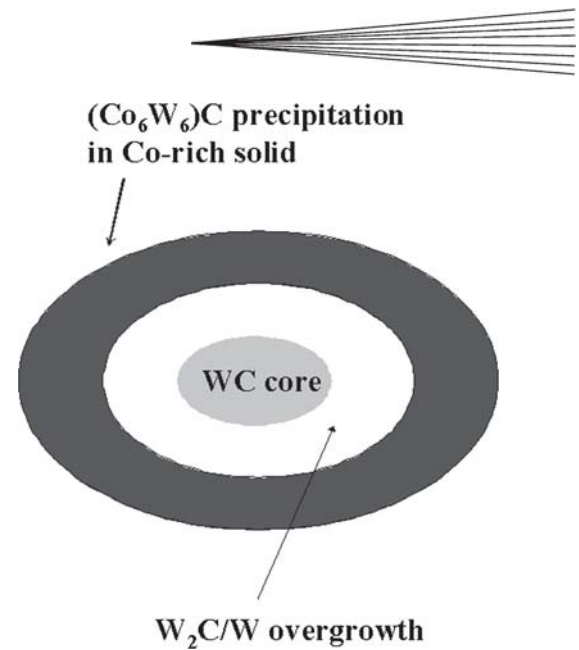
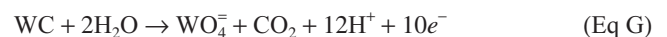
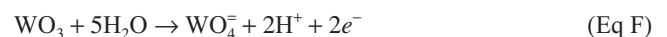
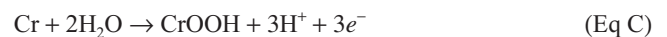
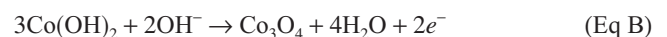


Fig. 21 Representation of possible W species in HVOF thermal spray coatings Sadangi (Ref 34)

has been devised to attempt to capture the parallel and sequential processes. The mechanisms are very complex, and different reactions can be occurring simultaneously at different areas of the surface.

The meaning of W species was suggested by Sadangi (Ref 34) (Fig. 21) showing formation of W and W_2C where the presence of the white contour around the hard phase after anodic polarization could also be related to W_2C . The corrosion would take place initially at the inner region where WC is the predominant phase and consequently affects W_2C , but as reported earlier (Ref 26), the XRD results for the coating presented in this work showed a low amount of $(Co_6W_6)C$ and W metal. The comment would be that the W metal formed would be present at the outer part of the W species and could also be in the matrix away from the WC/ W_2C species.

The reactions are summarized as follows, bearing in mind that the reactions could take place in a different order.



3.7 Effect of Corrosion on Erosion-Corrosion: General Implications

For large particles, it is likely that both the dissolution toward matrix and towards hard phase will take place to a certain degree

and then the particle will be removed either by losing support of the matrix or by physical effects of the jet under erosion-corrosion environments. For very small particles (less than 1 μm), the dissolution takes less time to complete and, as seen in post test analysis, the particle can be entirely chemically removed due to the high activity created by the higher surface area of small particles (Ref 22).

The reason some authors have detected the oxidation and dissolution of WC and some others did not is still not clear (Table 1). However the high dislocation density, which can be encountered in HVOF WC-based coatings (Ref 35) could perhaps be related to corrosion behavior of the materials as it is in stress cracking corrosion (Ref 36). Another important factor is the preferential corrosion, which seems to take place first in small particles; this could have been formed due to fracture of the relatively large particles upon the impact during the process as reported by Wirojanupatump et al. (Ref 37). In the HVOF process, the particle size distribution can be reduced due to the impact with the substrate increasing their surface area and the chemical activity of the particles.

4. Conclusions

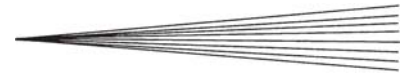
- The corrosion of WC-Co-Cr HVOF coatings is very complex and the rate increases with the temperature.
- WC in HVOF coatings dissolves as well as the cobalt-chromium matrix, leading to cobalt in solution.
- Chromium forms an oxide layer, which protects from dissolution and retards the corrosion.
- WC and Co go through an oxidation process before dissolution.
- The oxidation of WC to WO_3 makes the pH drop, accelerating the dissolution of cobalt.
- Where corrosion of hard phase occurs, leading to its removal, there are serious implications for when the coatings are used in corrosive-erosive environments.

Acknowledgments

The authors acknowledge the financial support from Greenhey Engineering, England and Weir Pumps Ltd., Glasgow, Scotland, for V.A.D.S.

References

1. R.C. Tucker Jr., *Thermal Spray Coatings, ASM Handbook, Vol. 5, Surface Engineering*, ASM International, 1994, p 497-509
2. V.A.D. Souza, A. Neville, L. Phillips, P.A. Smith, P. Gourdji, and H.W. Wang, Meeting the Challenges in Pump Durability by Advanced Surface Engineering, *Second International Symposium on Advanced Materials for Fluid Machinery, Institution of Mechanical Engineers Event Transactions*, Feb 26, Professional Engineering Publishing Limited, The Institution of Mechanical Engineers, London, UK, 2004, p 95-111
3. V.A.D. Souza and A. Neville, Corrosion and Synergy in a WC-Co-Cr HVOF Thermal Spray Coating - Understanding Their Role in Erosion-Corrosion Degradation, *Wear*, 2005, 259, p 171-180
4. R.J. Wood and S.P. Hutton, The Synergistic Effect of Erosion and Corrosion: Trends in Published Results, *Wear*, 1990, 140, p 387-394
5. M.M. Stack, S. Zhou, and R.C. Newman, Identification of Transitions in Erosion-Corrosion Regimes in Aqueous Environments, *Wear*, 1995, 186-187, p 523-532
6. A. Fan, J. Long, and Z. Tao, Failure Analysis of Impeller of a Slurry Pump Subjected to Corrosive Wear, *Wear*, 1995, 81-183, p 876-882
7. M. Matsumura, Erosion Corrosion of Metallic Materials in Slurries, *Corrosion Review*, 1994, 12, 3-4, p 321-340
8. A.M. Human and H.E. Exner, Electrochemical Behaviour of Tungsten-Carbide Hardmetals, *Mater. Sci. Eng.*, 1996, A209, p 180-191
9. A.M. Human, B. Roebuck, and H.E. Exner, Electrochemical Polarization and Corrosion Behaviour of Cobalt and Co (W,C) Alloys in 1 N Sulphuric Acid, *Mater. Sci. Eng.*, 1998, A241, p 202-210
10. C. Monticelli, A. Frignani, and F. Zucchi, Investigation on the Corrosion Process of Carbon Steel Coated by HVOF WC/Co Cermets in Neutral Solution, *Corros. Sci.*, 2004, 46, p 1225-1237
11. A. Trueman, D.P. Schweinsberg, and G.A. Hope, A Study of the Effect of Cobalt Additions on the Corrosion of Tungsten Carbide/Carbon Steel Metal Matrix Composites, *Corros. Sci.*, 1999, 41, p 1377-1389
12. E.J. Wentzel and C. Allen, The Erosion-Corrosion Resistance of Tungsten-Carbide Hard Metals, *Int. J. Refract. Met. Hard Mater.*, 1997, 15, p 81-87
13. H. Scholl, B. Hofman, and A. Rauscher, Anodic Polarization of Cemented Carbides of the Type [(WC,M);M = Fe, Ni or Co] in Sulphuric Acid Solution, *Electrochim. Acta*, 1992, 37 (3), p 447-452
14. M.H. Ghandelari, Anodic Behaviour of Cemented WC-6%Co Alloy in Phosphoric Acid Solutions, *J. Electrochem. Soc.*, 1980, 127 (10), p 2144-2147
15. W.J. Tomlinson and C.R. Linzell, Anodic Polarization and Corrosion of Cemented Carbides with Cobalt and Nickel Binders, *J. Mater. Sci.*, 1988, 23, p 914-918
16. S. Imasato, S. Sakaguchi, and Y. Hayashi, Corrosion Behaviour of WC-Ni-Cr Cemented Carbide in NaOH Solution, *Nippon Tungsten Review*, 2000, 32, p 8-16
17. M. Takeda, N. Morihiro, R. Ebara, and Y. Harada, Corrosion Behaviour of Thermally Sprayed WC Coating in Na_2SO_4 Aqueous Solution, *Mater. Trans.*, 2002, 43, 11, p 2860-2865
18. A. Warren, A. Nylund, and I. Oleford, Oxidation of Tungsten and Tungsten Carbide in Dry and Humid Atmospheres, *Int. J. Refractory Metals Hard Mater.*, 1996, 14, p 345-353
19. J.D. Voorhies, Electrochemical and Chemical Corrosion of Tungsten Carbide (WC), *J. Electrochem. Soc.: Electrochem. Sci. Technol.*, 1972, 119, 2, p 219-222
20. K.M. Andersson and L. Bergstrom, Oxidation and Dissolution of Tungsten Carbide Powder in Water, *Int. J. Ref. Metals Hard Mater.*, 2000, 18, p 121-129
21. B. Bozzini, G.P. De Gaudenzi, A. Fanigliulo, and C. Mele, Electrochemical Oxidation of WC in Acidic Sulphate Solution, *Corros. Sci.*, 2004, 46, p 453-469
22. I. Nikolov, G. Papazov, and V. Naidenov, Activity and Corrosion of Tungsten Carbide Recombination Electrodes during Lead/Acid Battery Operation, *J. Power Sources*, 1992, 40, p 333-340
23. I. Nikolov and T. Vitanov, The Effect of Method of Preparation on the Corrosion Resistance and Catalytic Activity during Corrosion of Tungsten Carbide., I. Corrosion Resistance of Tungsten Carbide in Sulfuric Acid, and II. Changes in the Catalytic Activity of Tungsten Carbides during the Corrosion Process, *J. Power Sources*, 1980, 5, p 273-291
24. "G5-Reference Test Method for Making Potentiostatic and Potentiodynamic Anodic Polarisation Measurements," "G59-Practice for Conducting Potentiodynamic Polarisation Resistance Measurements," Annual Book of ASTM Standards 2002, Section 03, 03-02, G 5 and G 59, ASTM, 2002
25. V.A.D. Souza and A. Neville, Corrosion of WC-Co-Cr Cermet Coatings Using In-Situ Atomic Force Microscopy, Advancing the Science & Applying the Technology, B.R. Marple, and C. Moreau, Ed., *Proceedings of 2003 International Thermal Spray Conference ITSC*, 5-8 May, Orlando, FL, ASM International, 1, 2003, p 395-404
26. V.A.D. Souza, "Corrosion and Erosion-Corrosion of WC-based Cermet Coatings—A Kinetic and Mechanistic Study," Ph.D. Thesis, Heriot-Watt University, Scotland, August 2004
27. R.D. Armstrong, K. Edmondson, and R.E. Firman, The Anodic Dissolution of Tungsten in Alkaline Solution, *J. Electroanal. Chem.*, 1972, 40 (1), p 19-28
28. M.S. El-Basoumy, F.E.T. Heikel, and M.M. Hefny, On the Electro-



- Chemical-Behavior Of Tungsten Corrosion Behavior Of Tungsten in Buffer Solutions as Revealed by Potential and Impedance Measurement at Open Circuit Potential, *Corrosion*, 1981, 37, p 175-178
29. M. Anik and K. Osseo-Asare, Effect of pH on the Anodic Behavior of Tungsten, *J. Electrochem. Soc.*, 2002, 149, 6, p B224-B233
30. S. Sutthiruangwong, G. Mori, and R. Kusters, Passivity and Pseudopassivity of Cemented Carbides, *Int. J. Refract. Met. Hard Mater.*, 2005, 23, p 129-136
31. I. Milosev and H-H. Strehblow, The Composition of the Surface Passive Film Formed on CoCrMo Alloy in Simulated Physiological Solution, *Electrochimica Acta*, **48**, Issue 19, (2003), p 2767-2774
32. T. Ohtsuka and N. Sato, Two-Layer Formation of Passivating Films on Cobalt in Neutral Solution, *J. Electrochem. Soc.*, 1981, 128, 12, p 2522-2528
33. M. Pourbaix, *Atlas of Electrochemical Equilibria in Aqueous Solutions*, NACE, Cebelcor, Houston, TX, 1974
34. R.K. Sadangi, G. Skandan, and B.H. Kear, Factors Controlling Decarburisation in HVOF Sprayed Nano-WC/Co Hardcoatings, *Scripta Mater.*, 2001, 44, p 1703-1707
35. D.G. McCartney, A. Stewart, and P.H. Shipway, Micro Structural Evolution in Thermally Sprayed WC-Co Coatings: Comparison Nanocomposite and Conventional Starting Powders, *Acta Mater.*, 2000, 48, p 1593-1604
36. T. Magnin, A. Chambreuil, and B. Bayle, The Corrosion-Enhanced Plasticity Model for Stress Corrosion Cracking in Ductile fcc Alloys, *Acta Mater.*, 1996, 44, 4, p 1457-1470
37. S. Wirojanupatump, P.H. Shipway, and D.G. McCartney, The Influence of HVOF Powder Feedstock Characteristics on the Abrasive Wear Behaviour of Cr_xC_y -NiCr Coatings, *Wear*, 2001, 249, p 829-837